HHS Public Access

Author manuscript

Int Conf Manip Autom Robot Small Scales. Author manuscript; available in PMC 2023 September 02.

Published in final edited form as:

Int Conf Manip Autom Robot Small Scales. 2022 July ; 2022: . doi:10.1109/marss55884.2022.9870486.

Cellular Manipulation Using Rolling Microrobots

David Rivas[1], **Sudipta Mallick**[1], **Max Sokolich**[1], **Sambeeta Das**[1]

[1]Department of Mechanical Engineering, University of Delaware

Abstract

Many biomedical applications, such as targeted drug delivery or cell manipulation, are well suited for the deployment of microrobots, untethered devices that are capable of carrying out tasks at the microscale. One biocompatible means of driving microrobots relies on magnetic actuation. In particular, microrobots driven using rotating fields rather than magnetic field gradients are especially practical for real-word applications. Many biological applications involve enclosed environments, such as blood vessels, in which surfaces are abundant, therefore, surface rolling is a particularly pertinent method of transportation. In this paper we demonstrate manipulation and transportation of cells using two types of magnetically driven rolling microrobots. We find that the microrobots are able to manipulate the cells by physically pushing or by first adhering to the cells and then carrying them. Microrobots spinning at high rates also can transport cells via the induced fluid flows.

Keywords

cell manipulation; microrobots

I. INTRODUCTION

Microrobots have been envisioned to be useful tools in biomedical applications such as targeted drug delivery or cell manipulation [1]. Most microrobots constructed so far involve the use of toxic chemicals or light-based actuation mechanisms that are unable penetrate inside the body. Magnetic robots have been the subject of sustained interest in the biomedical field due to their ability to be steered in biological samples without harming cells or tissues[2]. Typically, these microrobots are driven by magnetic gradients which create a magnetic force on the microrobot. However, at the small scales relevant for microrobotics, it is generally harder to drive microrobots using magnetic gradients compared to rotating magnetic fields [2], [3], which makes a microrobot that can propel by magnetic torques an intriguing alternative.

One type of microrobot that is designed to move under rotating magnetic fields is a helical microrobot, which propels in a similar way as a bacterial flagella [2]. Another type of microrobot that is also propelled by rotating magnetic fields is a magnetic rolling microrobot, which is generally rolled on a solid surface [4], [5], [6], [7], [8], [9], [10]. Because these microrobots move at boundaries where fluid flow is reduced, they have been shown to move effectively even in the presence of fluid flows [11], [12], [13], [14]. Rolling

microrobots are also able to manipulate or transport cells [15], [4], making them promising candidates for other biomedical applications.

In this work, we use silica based microrobots in an environment densely populated by cells in which we move the microrobots by magnetic rolling (see Fig. 1). The microrobots can be moved to specific cells and can manipulate the cells by pushing. The Microrobots sometimes adhere to the cells, enabling the microrobot to carry the cells from one area to another. In addition, we also show that buoyant microrobots can be rolled at the top surface of an enclosed chamber as well as at an air-liquid interface. This could be useful in applications in enclosed systems such as blood vessels, or at air-liquid interfaces which is relevant in the pulmonary system [16], for example.

II. MOTIVATION AND RELATED WORK

In general, the field of cell biology could benefit greatly from a versatile, selective, and quick mode of cellular manipulation and cargo delivery for a variety of applications and basic research[17], [18]. From an engineering standpoint, the manipulation and relocation of cells could lead to the development of artificial organ systems and high-fidelity cell sorting, driving advancements in biotechnology and medicine. Additionally, biologists could selectively position and rotate cells to study advanced microscopy, intercellular communication pathways, differences in molecular recognition, and targeted, selective delivery of interesting biomolecules [19], [20], [21]. Given these advanced, potentially transformative applications, methods of manipulating single cells are of intense interest to biologists and roboticists alike. While optical and magnetic tweezers are incredibly effective systems to manipulate micro and nanoscale objects, their force output is low [22], [23], [24]. They are also exceedingly expensive and difficult to assemble, and manipulating single cells directly with optical tweezers typically damages and kills them [25]. Practically, these systems have been augmented such that the surfaces are functionalized with biochemicals which have targeted functionalities. For instance, colloids driven by magnetic transporters have been functionalized with antibodies to test binding affinity with inflammatory proteins [26]. In a similar fashion, optical traps have been used to test T cell receptor affinity [27]. In both cases, the microrobots have an integrated mechanochemical action which is used to assess cellular activity.

To overcome these issues, many teams are focusing on perfecting methods for manipulating and interfacing with single mammalian cells without causing damage or changing the cell's morphology or chemistry. Dai *et al.* have shown that microbubbles can be generated and controlled optothermally, allowing them to quickly and efficiently manipulate a variety of microscale objects[28]. Wang *et al.* have demonstrated complex, even intracellular manipulation of cells via magnetic manipulation of microbeads[29] with a complex magnetic tweezer setup. Others have attempted to use acoustically-actuated robots for biomedical applications[30], [31] although motion is typically limited or requires high acoustic powers that could damage cells and generate undesirable bulk acoustic streaming and pressure nodes.

In contrast, magnetically driven microrobots provide the advantage of using a biocompatible driving mechanism with a large penetration depth. Therefore, they are attractive candidates for cellular transportation or manipulation. Our system utilizes rolling microrobots which can be rolled on surfaces and interfaces using a 3D electromagnetic coil setup (see Fig. 2), making them especially suitable for biological environments. Specifically, we envision that they could be beneficial in applications requiring maneuvering in blood vessels, such as removal of obstructions, or in cellular manipulation or delivery, such as cell sorting or biological research experiments as described above.

III. MATERIALS AND METHODS

A. Fabrication of microrobots

The microrobots were made using 45–85 μm diameter hollow silica spheres with a thin TiO_2 coating (Cospheric) and 20 μm diameter silica spheres with amine functionality (Nanocs, Cat. No. Si20u-AM-1). The spheres were coated with nickel by e-beam deposition to make them magnetic (see Fig. 3). Both the hollow and the solid silica spheres were coated with 100 nm of nickel, although the deposition was performed at a 70 degree glancing angle in the case of the silica spheres (see Fig. 3) which generally reduced the surface area that was coated. Fig. 4 shows SEM images of the coated microrobots. Note that the magnetic moment of the spheres that have only a partial Ni coating tends to point in a direction tangent to the coated surface, whereas the spheres that are half-coated in Ni produce a magnetic moment that points normal to the surface, as can be seen from the alignment of the microrobots when a magnetic field is applied (see Video 1).

B. Mammalian cells

Mammalian cells served as model cells for manipulation by the microrobots. Human breast cancer cells (MCF-7) and Hepatocellular Carcinoma cells (HepG2) cells were gifted by Richard West (Associate Scientist at Flow Cytometry Core Facility). Cells were cultured in Dulbecco's Modified Essential Medium (DMEM, Gibco, BenchStable, USA) media with 5% CO_2 and maintained at 37 °C in an incubator. All experiments were performed after third passage of cells. Cells were washed with Dulbecco's phosphate buffer (DPBS, Gibco, BenchStable, USA) and trypsinized to detach cells from the culture dish. All experiments were carried out with these single cells. The microrobots were mixed with cells and their movement and manipulation of the cells was recorded.

Experiments in which the cytocompatibility of the microrobots was measured were performed by mixing the microrobots with the cells prior to incubation. For the incubation with the cracked hollow silica microrobots, the microrobots were broken by using a pipette tip to push them against the side of the vial.

Quantitative cell death was assessed by Trypan blue viability assay. The cells were collected in the media and after trypsinization. Then, the cells were centrifuged and suspended in phosphate buffered saline (PBS). The cells were then stained using 0.4% trypan blue and counted by a cell counter (Nexcelom Cellometer Vision Trio Cell Profiler). Cells (before

trypsinization) were observed under a microscope for morphology analysis, followed by Trypan blue staining to quantitatively assess cell viability after 24 hours.

C. Experimental Setup

A 3D magnetic field system (see Fig. 2) was used to apply rotating magnetic fields in the xz, or yz planes for magnetic rolling. The system consists of four electromagnets arranged orthogonally in the xy plane and a pair of Helmholtz coils positioned beneath and above the viewing plane for applying z fields. Magnetic field strengths of approximately 5 mT were used in the experiments. The magnetic field strengths from each of the coils was controlled using custom matlab or python code which produced digital signals that were used to modulate the current sent to each of the coils. To apply rotating magnetic fields, discrete sinusoidal signals were sent to each coil, with a 90 degrees phase difference between the two pairs of orthogonal electromagnets that corresponded to the desired rotation axis. For example, to apply a rotating field in the xz plane, the x-axis current was set as $A\cos(2\pi ft)$ and the z-axis as $A\sin(2\pi ft)$, with A the magnitude and f the frequency.

Experiments were conducted on an Axiovert 200 inverted microscope with a Amscope MU903–65 camera. The microrobots were observed either on a glass slide or within an enclosed chamber (Grace Bio-Labs SecureSeal Hybridization Chamber).

IV. RESULTS AND DISCUSSION

The microrobots could be rolled by applying rotating magnetic fields either in the xz or yz planes, which resulted in the translation of the microrobots in the y or x directions, respectively. Microrobots could be moved both on the solid substrate as well as at the air-liquid interface (see Video 1 and Video 2 and Fig. 6). The direction of motion at the air-liquid interface is the same as that on the solid surface for a given rotating field orientation, which can be explained by the larger drag on the bottom of the microrobot compared to that at the top in both cases. Buoyant microrobots were also rolled on the top surface of a sealed chamber, which results in the microrobot translating in the opposite direction (see Video 4).

The speed of the microrobots could be tuned by varying the magnetic field rotation frequency, ν. Figure (6) shows the measured speed of the solid silica and hollow microrobots (both on the glass substrate and at the air-liquid interface) as a function of rotating magnetic field frequency. As can be seen from the plot, the microrobot speed increased with frequency approximately linearly, as expected for a rolling object in which the speed is approximately equal to $2\pi Rf$, with R being the microrobot radius and f the rotation frequency. Note that, due to slip, the actual speed of a rolling microrobot in a fluid is reduced. From figure (4), one can see that the speed of the microrobots is considerably less than $2\pi Rf$, signifying that slip is significant. Interestingly, the hollow spheres moved faster at a given frequency at the air-liquid interface than on the solid substrate, indicating that they experienced less slip at the interface.

Above a threshold frequency, the microrobot was unable to maintain synchronicity with the magnetic field and its speed decreased. The threshold frequency at which this occurs depends on the relative degree of magnetic torque compared to the amount of rotational

drag. We found that this threshold frequency depended on the size of the microrobot and the amount of nickel coating on its surface, but generally occurred above about 10 Hz.

The buoyant hollow microrobots were able to move at speeds of up to about 300 $\mu m/s$ at the air-liquid interface and about 125 $\mu m/s$ on the glass substrate, while the smaller silica microrobots attained speeds of around 75 $\mu m/s$ on the substrate (see Fig. 5). Due to the adhesive and physical interaction with the cells, the maximum microrobot speeds were typically reduced in environments containing cells.

At relatively high densities, the microrobots sometimes formed aggregates due to attractive magnetic dipole interactions. Video 3 shows an example of chains and clumps of microrobots which tumble end over end when a rotating field is applied. The chains tend to tumble rather than roll, due to their magnetic moment residing along their long axis and therefore aligning with the applied magnetic field. This behavior is similar to that previously observed for chains and clusters of paramagnetic spheres [32], [33].

Hollow microrobots would sometimes crack, resulting in them sinking to the bottom substrate. We used these microrobots to manipulate cells by rolling them to the cells and either pushing the cells or, in some cases, carrying the cells (see Video and Fig. 7). We found that single microrobots generally could push but usually could not carry the cells (see Video 8 and 10), while larger clumps of microrobots were more likely to “pick up” cells by rolling them into the cells and carrying the cells with them (see Video 6 and 7). Although both microrobots tended to adhere to the cells, the hollow microrobots were more effective at carrying the cells, possibly due to their larger size or different surface properties. We conjecture that the origin of the adhesion between the cells and the microrobots is due to an electrostatic attractive force or Van der Waals attraction. We found that spinning the large hollow microrobots at high frequency in the xy plane sometimes resulted in the cells detaching from the microrobots (see Video 9).

Microrobots that were rolled at high frequencies created flows in the fluid which resulted in the advective motion of the cells (see Video 8). These flows tend to carry cells that were behind the microrobot forward while pushing those in front of it farther away, similar to what one would expect from the flow field produced by a neutral squirmer. Such manipulation using fluid flow created by a rolling microrobot is similar to previous work in which a rotating rod created a vortex that trapped protein crystals near the rod, allowing them to be moved with the rod [34]. This is reminiscent of our observation, in which the flow fields created by a hollow microrobot rolling at high frequency caused the cells in near proximity to the microrobot to move with the microrobot, as shown in video 8.

A. Cytocompatibility

We also tested the cytocompatibility of the microrobots with the cells. The cytocompatibility of the rolling microrobots was assessed in both HepG2 and MCF-7 cells. Cells were incubated for 24 hours with silica, hollow TiO_2 coated silica, as well as cracked hollow TiO_2 coated silica microrobots that were broken before adding them to the culture medium. Fig. 8) shows brightfield images of the cells after incubation along with a control in which no microrobots were added. As can be seen in the images, cells preferentially attached to the

microrobots, therefore providing another method for loading the cells onto the microrobots for transport and delivery. We also find that cell morphology and growth patterns were intact for both types of cells, indicating that the microrobots are not toxic to the cells. Trypan blue staining was also performed to quantitatively assess cell viability. The results show that the microrobots are not toxic to the cells (see Fig. 9). We also tested the viability of the cells after manipulation by the microrobots. Figure 10 shows images of MCF-7 cells before and after manipulation, as well as Trypan blue staining results. The results show that the cells are still viable after manipulation.

V. CONCLUSION AND FUTURE WORK

We have demonstrated manipulation of cells by means of magnetically rolling microrobots, which shows promise as a robust means of motility in biological applications, such as in blood vessels. Aside from manipulation, our results show that the microrobots can be effectively navigated in an environment populated with cells, which is relevant to many biological systems. In the future, it could be interesting to explore microrobots with varying surface properties and determine what effect this has on the adhesion of the microrobots to the cells. Also, using these microrobots for cell manipulation or delivery in more realistic environments, as well as at air-liquid interfaces where relatively little work has been done, would be another avenue of exploration of interest.

This technique opens up a variety of opportunities for biologists and roboticists alike, allowing for quick microscale assembly and manipulation with high precision. We plan to use this technique for a variety of biological and robotics studies, from interrogations of interesting biological phenomena, to dynamic control of multiple robots via a computer-controlled magnetic field. We imagine this robot and successive nanoscale robots being utilized as cheaper, simpler replacements for intense, field-driven tweezing that could extend the capabilities of many studies and make them more accessible to researchers without the need for expensive, hard-to-use equipment.

Supplementary Material

Refer to Web version on PubMed Central for supplementary material.

ACKNOWLEDGEMENTS

The authors gratefully acknowledge the late Richard West for his help with the cell lines. This project was supported by the Delaware INBRE program, with a grant from the National Institute of General Medical Sciences – NIGMS (P20 GM103446) from the National Institutes of Health and the State of Delaware. This work was also supported by NSF grant OIA2020973. This content is solely the responsibility of the authors and does not necessarily represent the official views of NIH.

REFERENCES

[1]. Sitti M, Ceylan H, Hu W, Giltinan J, Turan M, Yim S, and Diller E, “Biomedical applications of untethered mobile milli/microrobots,” Proceedings of the IEEE, vol. 103, no. 2, pp. 205–224, 2015. [PubMed: 27746484]

[2]. Peyer KE, Zhang L, and Nelson BJ, “Bio-inspired magnetic swimming microrobots for biomedical applications,” Nanoscale, vol. 5, pp. 1259–1272, 2013. [Online]. Available: 10.1039/C2NR32554C [PubMed: 23165991]

[3]. Abbott JJ, Peyer KE, Lagomarsino MC, Zhang L, Dong L, Kaliakatsos IK, and Nelson BJ, "How should microrobots swim?" The International Journal of Robotics Research, vol. 28, no. 11–12, pp. 1434–1447, 2009. [Online]. Available: 10.1177/0278364909341658

[4]. Jeon S, Kim S, Ha S, Lee S, Kim E, Kim SY, Park SH, Jeon JH, Kim SW, Moon C, Nelson BJ, young Kim J, Yu S-W, and Choi H, "Magnetically actuated microrobots as a platform for stem cell transplantation," Science Robotics, vol. 4, no. 30, p. eaav4317, 2019. [Online]. Available: 10.1126/scirobotics.aav4317 [PubMed: 33137727]

[5]. Pieters R, Tung H-W, Charreyron S, Sargent DF, and Nelson BJ, "Rodbot: A rolling microrobot for micromanipulation," in 2015 IEEE International Conference on Robotics and Automation (ICRA), 2015, pp. 4042–4047.

[6]. Ali J, Cheang UK, Liu Y, Kim H, Rogowski L, Sheckman S, Patel P, Sun W, and Kim MJ, "Fabrication and magnetic control of alginate-based rolling microrobots," AIP Advances, vol. 6, no. 12, p. 125205, 2016. [Online]. Available: 10.1063/1.4971277

[7]. Jiang G-L, Guu Y-H, Lu C-N, Li P-K, Shen H-M, Lee L-S, Yeh JA, and Hou MT-K, "Development of rolling magnetic microrobots," Journal of Micromechanics and Microengineering, vol. 20, no. 8, p. 085042, jul 2010. [Online]. Available: 10.1088/0960-1317/20/8/085042

[8]. Bi C, Guix M, Johnson BV, Jing W, and Cappelleri DJ, "Design of microscale magnetic tumbling robots for locomotion in multiple environments and complex terrains," Micromachines, vol. 9, no. 2, 2018. [Online]. Available: https://www.mdpi.com/2072-666X/9/2/68

[9]. Bi C, Niedert EE, Adam G, Lambert E, Solorio L, Goergen CJ, and Cappelleri DJ, "Tumbling magnetic microrobots for biomedical applications," in 2019 International Conference on Manipulation, Automation and Robotics at Small Scales (MARSS), 2019, pp. 1–6.

[10]. Magdanz V, Gebauer J, Mahdy D, Simmchen J, and Khalil IS, "Sperm-templated magnetic microrobots," in 2019 International Conference on Manipulation, Automation and Robotics at Small Scales (MARSS), 2019, pp. 1–6.

[11]. Wu Z, Zhang Y, Ai N, Chen H, Ge W, and Xu Q, "Magnetic mobile microrobots for upstream and downstream navigation in biofluids with variable flow rate," Advanced Intelligent Systems, vol. n/a, no. n/a, p. 2100266, 2022. [Online]. Available: 10.1002/aisy.202100266

[12]. Alapan Y, Bozuyuk U, Erkoc P, Karacakol AC, and Sitti M, "Multifunctional surface microrollers for targeted cargo delivery in physiological blood flow," Science Robotics, vol. 5, no. 42, p. eaba5726, 2020. [Online]. Available: 10.1126/scirobotics.aba5726 [PubMed: 33022624]

[13]. Bozuyuk U, Alapan Y, Aghakhani A, Yunusa M, and Sitti M, "Shape anisotropy-governed locomotion of surface microrollers on vessel-like microtopographies against physiological flows," Proceedings of the National Academy of Sciences, vol. 118, no. 13, p. e2022090118, 2021. [Online]. Available: 10.1073/pnas.2022090118

[14]. Karle M, Wöhrle J, Miwa J, Paust N, Roth G, Zengerle R, and von Stetten F, "Controlled counter-flow motion of magnetic bead chains rolling along microchannels," Microfluidics and Nanofluidics, vol. 10, no. 4, pp. 935–939, 2011. [Online]. Available: 10.1007/s10404-010-0727-8

[15]. Lin Z, Fan X, Sun M, Gao C, He Q, and Xie H, "Magnetically actuated peanut colloid motors for cell manipulation and patterning," ACS Nano, vol. 12, no. 3, pp. 2539–2545, 2018, [Online]. Available: 10.1021/acsnano.7b08344 [PubMed: 29443501]

[16]. Upadhyay S and Palmberg L, "Air-Liquid Interface: Relevant In Vitro Models for Investigating Air Pollutant-Induced Pulmonary Toxicity," Toxicological Sciences, vol. 164, no. 1, pp. 21–30, 03 2018. [Online]. Available: 10.1093/toxsci/kfy053 [PubMed: 29534242]

[17]. Das S, Steager EB, Stebe KJ, and Kumar V, "Simultaneous control of spherical microrobots using catalytic and magnetic actuation," in 2017 International Conference on Manipulation, Automation and Robotics at Small Scales (MARSS), July 2017, pp. 1–6.

[18]. Das S, Steager EB, Hsieh M, Stebe KJ, and Kumar V, "Experiments and open-loop control of multiple catalytic microrobots," Journal of Micro-Bio Robotics, vol. 14, no. 1, pp. 25–34, 2018.

[19]. Dai C, Zhang Z, Lu Y, Shan G, Wang X, Zhao Q, and Sun Y, "Robotic orientation control of deformable cells," in 2019 International Conference on Robotics and Automation (ICRA), May 2019, pp. 8980–8985.

[20]. Lu Z, Zhang Xuping, Leung C, Esfandiari N, Casper RF, and Sun Y, "Automated cell manipulation: Robotic icsi," in 2011 IEEE International Conference on Robotics and Automation, May 2011, pp. 2540–2545.

[21]. Mhanna R, Qiu F, Zhang L, Ding Y, Sugihara K, Zenobi-Wong M, and Nelson BJ, "Artificial bacterial flagella for remote-controlled targeted single-cell drug delivery," Small, vol. 10, no. 10, pp. 1953–1957, 2014. [PubMed: 24616145]

[22]. Gao W, Dongliang and Ding, Nieto-Vesperinas M, Ding X, Rahman, Zhang T, Lim C, and Qiu C-W, "Optical manipulation from the microscale to the nanoscale: fundamentals, advances and prospects," Light: Science & Applications, vol. 6, no. 9, 2017.

[23]. Brzobohaty O, Karasek V, Oiler M, Chvatal L, Citmár T, and Zemánek P, "Experimental demonstration of optical transport, sorting and self-arrangement using a tractor beam," Nature Photonics, vol. 7, no. 123, pp. 156–160, 2013.

[24]. Petit T, Zhang L, Peyer KE, Kratochvil BE, and Nelson BJ, "Selective trapping and manipulation of microscale objects using mobile microvortices," Nano Letters, vol. 12, no. 1, pp. 156–160, 2012, [PubMed: 22111870]

[25]. Keloth A, Anderson O, Risbridger D, and Paterson L, "Single cell isolation using optical tweezers," Micromachines, vol. 9, no. 9, p. 434, 2018. [PubMed: 30424367]

[26]. Steager EB, Zern B, Sakar MS, Muzykantov V, and Kumar V, "Assessment of protein binding with magnetic microrobots in fluid," in 2013 IEEE International Conference on Robotics and Automation, May 2013, pp. 5502–5507.

[27]. Ong LS, Zhu H, Banik D, Guan Z, Feng Y, Reinherz EL, Lang MJ, and Asada HH, "A robotic microscope system to examine t cell receptor acuity against tumor neoantigens: A new tool for cancer immunotherapy research," IEEE Robotics and Automation Letters, vol. 4, no. 2, pp. 1760–1767, April 2019.

[28]. Dai L, Ge Z, Jiao N, Shi J, and Liu L, "Manipulation using microrobot driven by optothermally generated surface bubble," in 2019 International Conference on Robotics and Automation (ICRA), May 2019, pp. 219–224.

[29]. Wang X, Ho C, Tsatskis Y, Law J, Zhang Z, Zhu M, Dai C, Wang F, Tan M, Hopyan S, McNeill H, and Sun Y, "Intracellular manipulation and measurement with multipole magnetic tweezers," Science Robotics, vol. 4, no. 28, 2019.

[30]. Ahmed D, Baasch T, Jang B, Pané S, Dual J, and Nelson BJ, "Artificial swimmers propelled by acoustically activated flagella." Nano letters, vol. 16, pp. 4968–74, 2016. [PubMed: 27459382]

[31]. Louf J-F, Bertin N, Dollet B, Stephan O, and Marmottant P, "Hovering microswimmers exhibit ultrafast motion to navigate under acoustic forces," Advanced Materials Interfaces, vol. 5, no. 16, p. 1800425, 2018.

[32]. Morimoto H, Ukai T, Nagaoka Y, Grobert N, and Maekawa T, "Tumbling motion of magnetic particles on a magnetic substrate induced by a rotational magnetic field," Phys. Rev. E, vol. 78, p. 021403, Aug 2008. [Online]. Available: 10.1103/PhysRevE.78.021403

[33]. Sing CE, Schmid L, Schneider MF, Franke T, and Alexander-Katz A, "Controlled surface-induced flows from the motion of self-assembled colloidal walkers," Proceedings of the National Academy of Sciences, vol. 107, no. 2, pp. 535–540, 2010. [Online]. Available: 10.1073/pnas.0906489107

[34]. Pieters RS, Tung H-W, Sargent DF, and Nelson BJ, "Non-contact manipulation for automated protein crystal harvesting using a rolling microrobot," IFAC Proceedings Volumes, vol. 47, no. 3, pp. 7480–7485, 2014, 19th IFAC World Congress. [Online]. Available: https://www.sciencedirect.com/science/article/pii/S1474667016427916

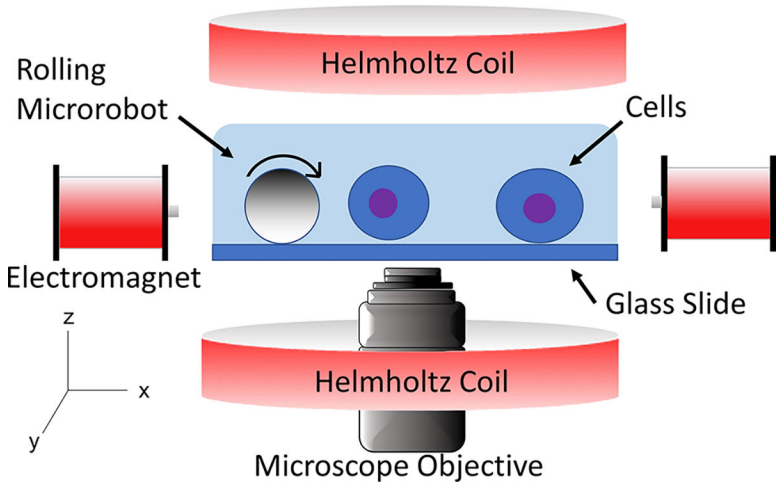

Figure 1.
(a) Schematic representation of the experimental setup.

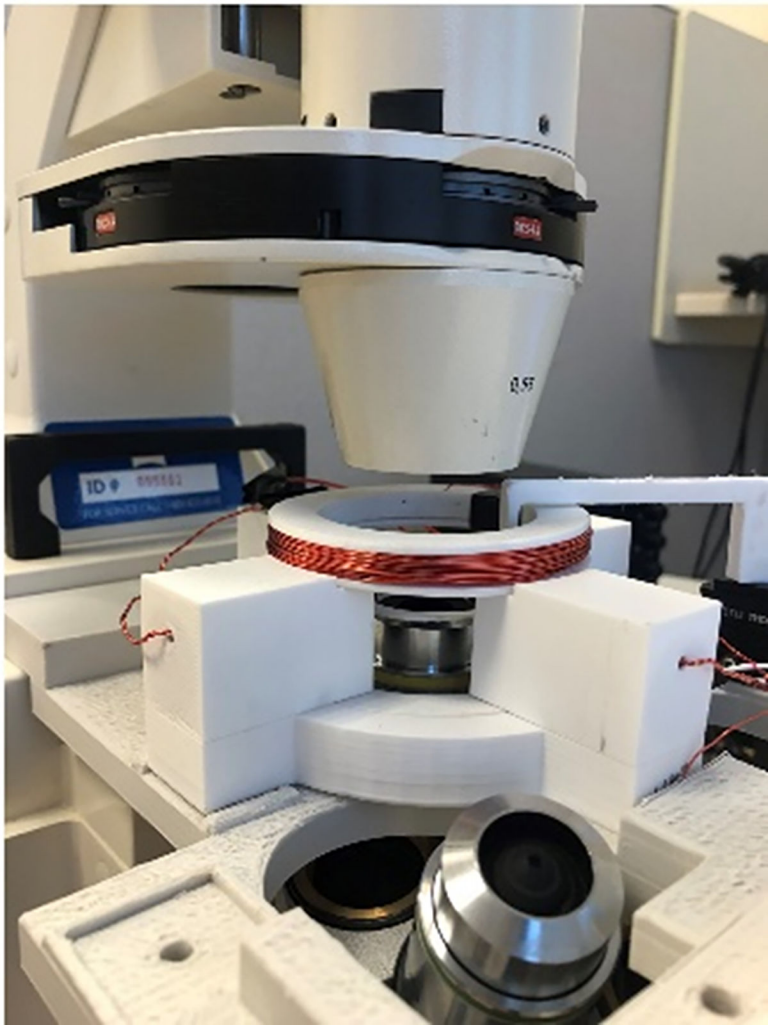

Figure 2.
Magnetic setup demonstrating the electromagnetic coils

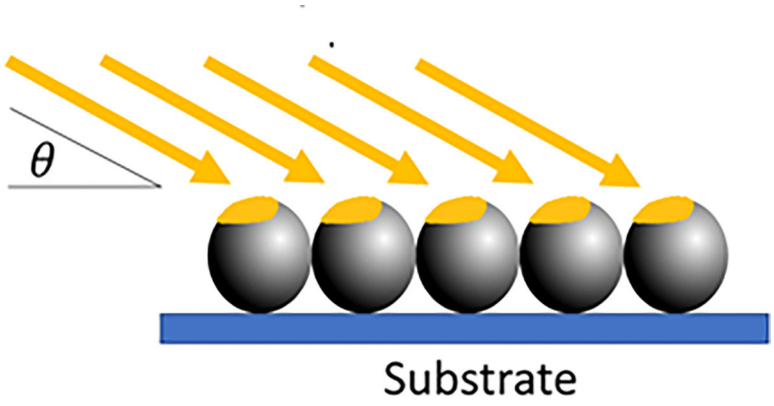

Figure 3.
Schematic of glancing angle deposition for the microrobots. Nickel vapor was deposited at a 70 degree angle for these microrobots

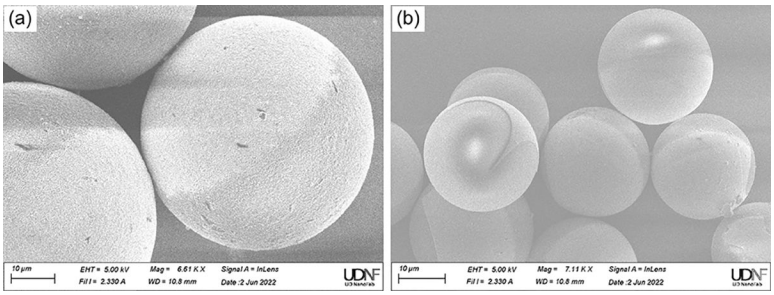

Figure 4.

(a) SEM images of the hollow spherical microrobots and (b) of the solid silica microrobots, both coated with a nickel layer.

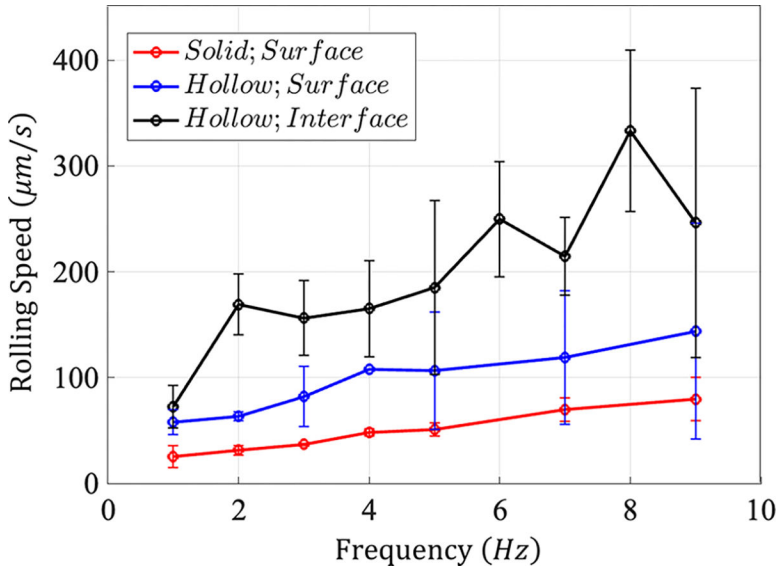

Figure 5.

(a) Microrobot speed versus frequency of 20 μm diameter silica solid spheres rolling on the glass substrate and ~70 μm diameter TiO2 hollow spheres on the substrate and at the air-liquid interface. Error bars correspond to standard deviations of multiple trials.

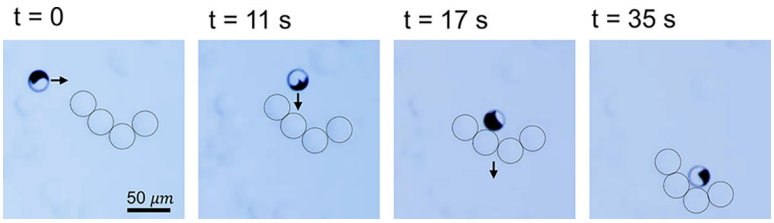

Figure 6.

A sequence of images showing a silica rolling microrobot pushing HepG2 cells. The cells that are manipulated by the microrobot are circled for visual aid.

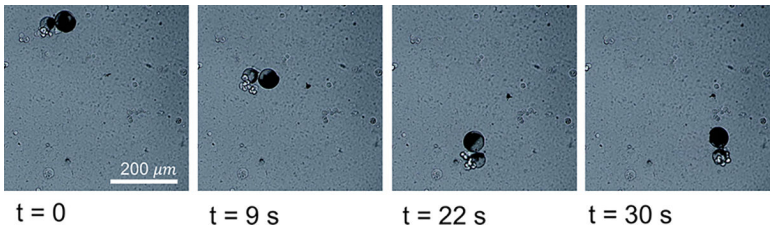

Figure 7.
Image sequence showing a pair of hollow rolling microrobots carrying MCF-7 cells.

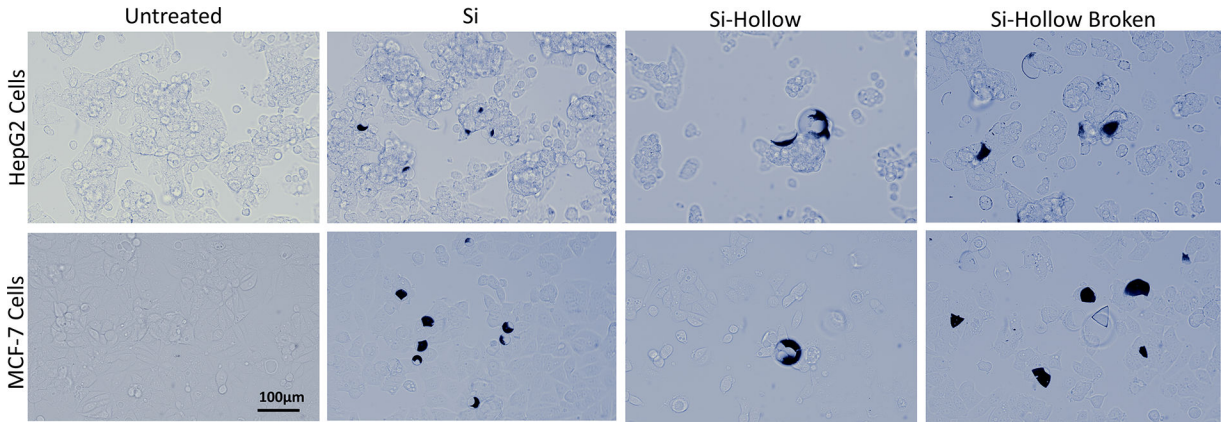

Figure 8.

Images of cultured MCF-7 and HepG2 cancer cells after 24 hours with (from left to right) no microrobots, silica microrobots, hollow TiO_2 coated silica microrobots, and cracked hollow TiO_2 coated silica microrobots. As can also be seen from the images, the cells preferentially attach to the microrobots during their growth.

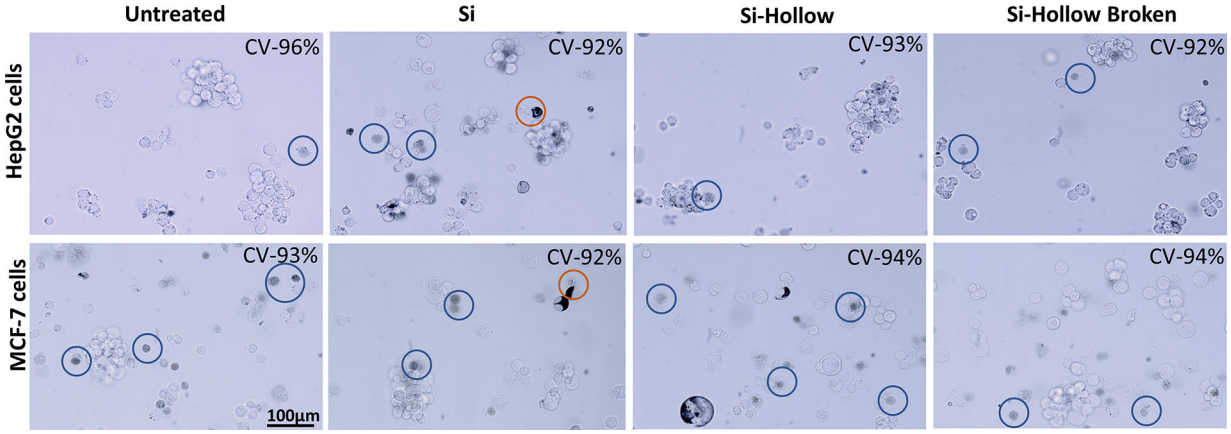

Figure 9.

Images of cultured MCF-7 and HepG2 cancer cells after 24 hours with (from left to right) no microrobots, silica microrobots, hollow TiO_2 coated silica microrobots, and cracked hollow TiO_2 coated silica microrobots. HepG2 and MCF-7 cells were observed under the microscope and trypan blue staining was performed to assess cell viability. Dead cells were shown in blue circles and live cells attached to MRs are shown in red circles. CV: Cell Viability.

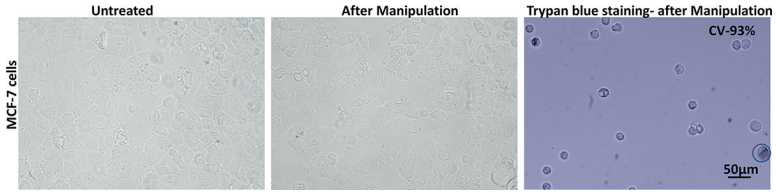

Figure 10.

MCF-7 cells were observed under the microscope after manipulation. The cell morphology of the cells which were manipulated by the microrobots was normal and indistinguishable from untreated cells. Trypan blue viability assay showed 93% viability after manipulation. Dead cells are shown in blue circles. CV: Cell Viability.